Pharmacological Reports 71 (2019) 319–329

Contents lists available at ScienceDirect

Pharmacological Reports

journal homepage: www.elsevier.com/locate/pharep

Original article

Astragaloside IV inhibits palmitate-mediated oxidative stress and fibrosis in human glomerular mesangial cells *via* downregulation of CD36 expression

Yong Su[a,b], Qingqing Chen[a], Keke Ma[a], Yinghui Ju[a], Tianjiao Ji[a], Zhongyuan Wang[a], Weizu Li[a,*], Weiping Li[a,c,*]

[a] *Key Laboratory of Anti-Inflammatory and Immunopharmacology, Ministry of Education, Department of Pharmacology, Anhui Medical University, Hefei 230032, Anhui, China*
[b] *Department of Pharmacy, The First Affiliated Hospital of Anhui Medical University, Hefei 230032, Anhui, China*
[c] *Anqing Medical and Pharmaceutical College, Anqing 246052, Anhui, China*

ARTICLE INFO

Article history:
Received 26 August 2018
Received in revised form 11 December 2018
Accepted 19 December 2018
Available online 21 December 2018

Keywords:
Palmitate
Astragaloside IV
CD36
Fibrosis
Oxidative stress

ABSTRACT

Background: The increased influx of free fatty acids (FFAs) into the kidney is a risk factor for diabetes nephropathy (DN). In the present study we investigated the effects of astragaloside IV (AS-IV) on FFA-induced lipid accumulation, oxidative stress, and activation of TGF-β1 signaling in human glomerular mesangial cells (HMCs).
Methods: A DN model was induced in Sprague Dawley rats by the administration of a high-fat diet and streptozocin, and HMCs were stimulated with palmitate. Lipid accumulation and FFA uptake were detected using Oil Red O and BODIPY^{TM} FL C_{16} staining, respectively. The expression levels of TGF-β1, p-Smad2/3, FN, Col4 A1, NOX4, p22phox, and CD36 were evaluated by western blotting or immunofluorescence/immunohistochemistry. The level of reactive oxygen species (ROS) was detected using 2′,7′-dichlorofluorescein diacetate and dihydroethidium.
Results: Exposure to palmitate induced marked lipid accumulation in HMCs, whereas co-treatment with AS-IV significantly attenuated this phenomenon. Moreover, AS-IV suppressed palmitate-induced expression of TGF-β1, p-Smad2/3, FN, Col4 A1, NOX4, and p22phox, in addition to ROS production. Notably, AS-IV reduced the palmitate-induced expression of CD36 in HMCs and DN rats. Treatment of HMCs with the CD36 inhibitor, sulfo-*N*-succinimidyl oleate (SSO), significantly attenuated FFA uptake, oxidative stress, and fibrosis. Nevertheless, the combined use of SSO and AS-IV did not enhance the efficacy.
Conclusion: AS-IV inhibited palmitate-induced HMCs oxidative stress and fibrosis *via* the downregulation of CD36 expression, mediating FFA uptake and lipid accumulation.

Introduction

Diabetic nephropathy (DN) remains the major global cause of end-stage renal disease (ESRD) [1,2]. DN is characterised by ultrastructural alterations in glomeruli, which are mainly caused by augmented deposition of extracellular matrix (ECM) proteins such as fibronectin (FN) and collagen IV (Col IV). These alterations are attributed to the abnormal stimulation of glomerular mesangial cell (MC), which induces increased secretion of transforming growth factor β1 (TGF-β1). Subsequently, TGF-β1 binds to the transmembrane type II TGF-receptor (TRII) and upregulates FN and Col IV expression. Oxidative stress plays an important role during this pathophysiological process. Increasing evidence suggests that oxidative stress is associated with multiple molecular events in DN [3] due to metabolic changes [4,5]. Certain studies have implicated oxidative stress in ultrastructural alterations in glomeruli; excessive reactive oxygen species (ROS), the product of oxidative stress, have been shown to affect TGF-β1 signaling and accelerate deposition of ECM [6].

Nicotinamide adenine dinucleotide phosphate (NADPH) oxidase, one of the main sources of ROS in MC, consists of two membrane-associated subunits, p22phox and gp91phox [7,8], which constitute its catalytic core. However, NOX4 is the most abundant NOX isoform in the renal system and is highly expressed

* Corresponding authors.
E-mail addresses: liweizu@126.com (W. Li), lwp19@126.com (W. Li).

https://doi.org/10.1016/j.pharep.2018.12.008
1734-1140/

in MC. Moreover, NOX4derived ROS is the major contributor to renal morphological changes and functional abnormalities in DN [3,6,9,10], and inhibition of NOX4 protects mesangial expansion in DN [10].

In addition to hyperglycemia, increased plasma free fatty acids (FFAs) are detected in type 2 diabetes (T2DM) and have been further identified as a risk factor [11,12]. However, recent studies have shown that excessive FFAs are associated with DN [13] by triggering endoplasmic reticulum stress, which leads to podocyte apoptosis [14,15]. Stimulation of HMCs with FFAs has been shown to result in the upregulation of TGF-β1 and FN expression *in vitro* [16]. Moreover, FFAs are a potent inducer of ROS in a number of cell types including renal tubular epithelial cell [11,17]. The pathophysiological changes caused by FFAs are closely related to its absorption. CD36 is one of the major transporters of FFAs uptake. Previous research suggests that FFAs-induced cell damage may depend on CD36-mediated FFAs uptake [11]. We speculated that FFAs may play an important role in the induction of oxidative stress and fibrosis in HMCs, and the mechanism may be related to CD36 expression and function.

Astragaloside IV (AS-IV, 3-O-β-D-xylopyranosyl-6-O-β-D-glucopyranosyl- cycloastragenol), a purified small saponin, is extracted from *Radix Astragali*, and is one of its major active substances with comprehensive biological properties, including antioxidant, anti-inflammatory, and immunomodulatory efficacies [7,18]. Our previous studies have confirmed the protective effects of AS-IV on HG-induced HMCs oxidative stress [7]. Recently, it has been proven that AS-IV protects hepatocytes from the endoplasmic reticulum stress and lipid accumulation caused by FFAs [19].

Despite previous study showing that FFA promotes HMCs fibrosis, the underlying mechanism remains unclear. We speculated that it may be related to increased CD36-mediated FFA uptake, leading to oxidative stress and fibrosis. In the present study, we further investigated the effect and underlying mechanism of AS-IV on FFA-mediated HMCs injury to define whether CD36 is implicated in the renoprotective effect of AS-IV in palmitate-treated HMCs and high-fat diet and streptozocin-induced DN rats.

Materials and methods

Reagents

Both 2′,7′-dichlorofluorescein diacetate (DCFH-DA) and dihydroethidium (DHE) were obtained from Beyotime Biotechnology (Shanghai, China). Astragaloside IV (AS-IV) was purchased from Nanjing Zelang Medical Technology Co., Ltd. (Nanjing, China; purity > 98%, HPLC). Primary p-Smad2 (S465 + S467) and p-Smad3 (S423 + S425) antibody was obtained from Wanleibio Co., Ltd. (Shenyang, China). The TGF-β1 antibody was purchased from Abcam (Cambridge, UK) and the NOX-4, P22, and Col4 A1 antibodies from Bioworld Co., Ltd. (Louis Park, USA), and the CD36 antibody from Bioss Co., Ltd (Beijing, China). FN was bought from Immunoway (Plano, USA), and the β-actin antibody from Zhongshan Golden Bridge Biotechnology Co., Ltd. (Beijing, China). FFA-free bovine serum albumin (BSA) was obtained from Yesen Co., Ltd (Shanghai, China). PA and sulfo-*N*-succinimidyl oleate (SSO) were purchased from Sigma (St. Louis, MO, USA), and BODIPY^{TM} FL C_{16} from Thermo Fisher Scientific (Rockford, IL, USA).

Animals and DN model establishment

Male Sprague-Dawley rats (200 ± 20 g) were purchased from the Shandong Animal Centre (Shandong, China). The present study was approved by the Institutional Ethics Committee of our University (No. LLCC20180177) and carried out in accordance with the National Institutes of Health guidelines. After one week of adaptive feeding, the rats were randomly divided into two groups: the Control group (standard diet, n = 6) and the HFD group (high-fat diet). The Control group received a standard diet and the HFD group were fed a high-fat diet consisting of 8% lard, 10% yolk powder, 18% sucrose, and 0.5% sodium cholate (Xietong Co., Ltd, Jiansu, China) for 6 weeks [20]. Subsequently, diabetes was induced by intraperitoneal injection of streptozocin (35 mg/kg, Sigma) in the HFD group, and the Control group received an equal volume of saline. Rats with randomly assessed blood sugar levels greater than 16.7 mmol/L were considered diabetic and were selected for participation in the study 72 h later. These HFD-fed rats were divided into four groups: the DN group and the AS—IV (20, 40, and 80 mg/kg/d, intragastric administration) treatment groups (n = 8). All animals were humanely sacrificed two months later. Serum samples were collected for biochemical analysis. The left kidneys were stored at -80 °C for western blotting, and the right kidneys were embedded in paraffin for immunohistochemical analysis.

Palmitate-BSA preparation

Palmitate (PA) was prepared according to the published method [15,21]. Briefly, sodium palmitate (27 mM) was dissolved in distilled water (DW) at 70 °C for 30 min. BSA (30%) was also dissolved in DW at 55 °C for 30 min. Subsequently, the dissolved PA solution was added dropwise to the BSA solution and stored as a stock (13.5 mM) at 4 °C until use. The molar ratio of PA to BSA was maintained at 6:1 [22].

HMCs culture and treatment

HMCs were obtained from the Modern Analysis and Testing Centre of Central South University (Changsha, China) and maintained in DMEM (5.6 mM glucose) supplemented with 10% FBS, 100 μg/mL penicillin, and 100 μg/mL streptomycin at 37 °C in an atmosphere containing 5% CO_2. PA treatment was performed by culturing the cells in DMEM containing 200 μM PA for 24 h. The control for PA was DMEM containing 0.2% BSA. To investigate the protective effects of AS-IV, cells stimulated with PA were treated with AS-IV (20, 40, 80 μM) and/or SSO (250 μM).

Western blotting

Western blotting was performed as described in our previous study [23]. Briefly, the cells or tissues were lysed with cold lysis buffer containing both protease (PMSF) and phosphatase inhibitors. Equal amounts of protein extracts were separated by SDSPAGE and transferred to PVDF membranes. Following blocking in 5% skim milk, the membranes were incubated overnight at 4 °C with the appropriate primary antibodies (TGF-β1, NOX4, p-Samd2/3, p22phox, FN, Col4 A1, and CD36 at 1:500, and β-actin at 1:2000). The following day, membranes were rinsed three times with TBST and incubated with the respective secondary antibodies (1:10,000) for 1 h at room temperature. The protein bands were captured using a Bioshine ChemiQ 4600 Min. Chemiluminescence imaging system (Ouxiang Co., Ltd, Beijing, China). The optical density of each band was quantitated using the ImageJ software and normalised to the intensity of β-actin.

Measurement of intracellular ROS generation

The generation of intracellular ROS was measured using the membrane-permeable indicators, DCFH-DA and DHE. Cells were seeded in 24-well plates at a density of 1×10^5 cells/well. Following stimulation with PA, cells were loaded with DCFH-DA or DHE (10 μM) in serumfree DMEM at 37 °C for 30 min in the dark. Subsequently,

the intracellular ROS content was observed using a fluorescence microscope (BX-51, Olympus Co., Ltd. Japan). The mean fluorescence intensity for each group of cells was determined using the Image-Pro Plus 6.0 analysis system.

Immunofluorescence staining

HMCs cultured on 24well plates were washed three times with PBS and fixed with 4% paraformaldehyde for 10 min. Subsequently, cells were permeabilised with 0.5% Triton X-100 for 30 min, followed by blocking with 5% BSA for a further 60 min. Incubation with primary antibodies against FN (1:200) or CD36 (1:50) was performed overnight at 4 °C, followed by incubation with the respective secondary antibodies. Cells were then washed and stained with Hoechst 33,258 for 5 min.

Measurement of FFA uptake

The BODIPY™ lipid probe was used to measure FFA uptake. HMCs cultured on 24-well plates were incubated with BODIPY™ FL C_{16} (2.5 μM) dissolved in serum-free DMEM at 37 °C for 10 min, followed by observation under a fluorescence microscope.

Statistical analysis

Data were analysed using GraphPad Prism 6 and are presented as the mean ± standard deviation (SD). Statistical analysis was performed using one-way analysis of variance (ANOVA) followed by Tukey's test to compare differences among groups or a *t*-test to compare differences between two groups. A p value < 0.05 is considered statistically significant.

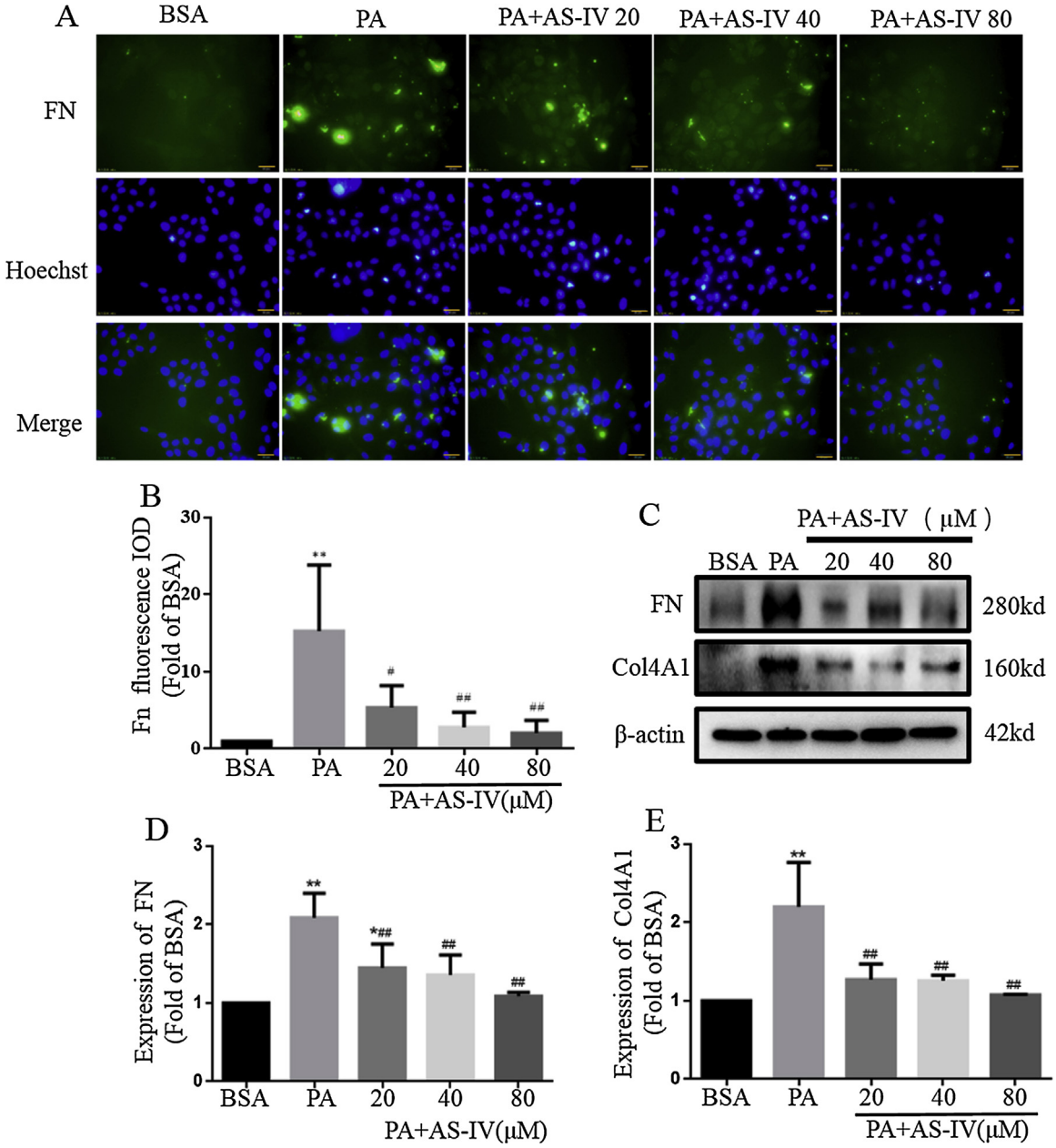

Fig. 1. AS-IV suppresses PA-induced FN and Col4 A1 expression in HMCs. (A) FN expression was detected by immunofluorescence (400×, bar = 20 μm). (B) Fluorescence intensity analysis of FN expression. (C) FN and Col4 A1 expression levels were detected by western blotting. (D) and (E) Densitometric analysis of FN and Col4 A1 expression. Data are expressed as the mean ± SD of three independent experiments. $^{*}p < 0.05$, $^{**}p < 0.01$ as compared with BSA; $^{\#}p < 0.05$ $^{\#\#}p < 0.01$ as compared with PA.

Results

AS-IV inhibits PA-induced HMCs fibrosis

HMCs were exposed to PA (200 μM) for 24 h to induce fibrosis, and the treatment groups were co-administered AS—IV at various concentrations, and the expression of FN was subsequently detected by immunofluorescence. The results show that FN expression increased significantly following stimulation with PA; however, administration of ASIV at a concentration of 20–80 μM led to significant inhibition of FN expression (Fig. 1A and B). Expression levels of FN and Col4 A1 (alpha-1 chain of COL4) were determined by western blotting. It can be seen that AS—IV inhibited PA-mediated upregulation of FN and Col4 A1 expression (Fig. 1C and D). Furthermore, we examined the expression levels of TGF-β1 and p-Smad2/3, which were found to be elevated following exposure to PA; however, ASIV inhibited the activation of the TGF-β1/Smad2/3 pathway (Fig. 2).

AS-IV suppresses PA-induced HMCs oxidative stress

We examined the effects of AS-IV on PA-induced intracellular ROS generation using DCFH-DA and DHE fluorescent probes. As demonstrated in Fig. 3, HMCs stimulated with PA for 24 h showed a significant increase in ROS generation as compared with those stimulated with BSA. Moreover, administration of 20–80 μM ASIV markedly decreased ROS generation (Fig. 3A–D). Subsequently, we evaluated the effect of ASIV on NOX4 and p22phox expression levels, which were found to be significantly upregulated by PA stimulation; however, treatment with 20–80 μM ASIV markedly downregulated expression (Fig. 3E–G).

AS-IV attenuates PA-induced HMCs lipid accumulation and CD36 expression

Previous studies have shown that PA induces intracellular lipid accumulation, which in turn causes cells oxidative stress and fibrosis [24–26]; therefore, intracellular neutral lipid accumulation was detected using Oil Red O staining. As shown in Fig. 4, intracellular lipid accumulation increased when HMCs were stimulated with PA for 24 h, while treatment with 20–80 μM ASIV inhibited this intracellular lipid accumulation in a dose-dependent manner (Fig. 4A and B). Subsequently, we examined the effect of ASIV on the expression of CD36. Consistent with the experimental results of the Oil Red O staining, PA stimulation for 24 h significantly upregulated the expression of CD36; however, 20–80 μM AS-IV markedly attenuated this expression (Fig. 4 C–F).

Inhibition of CD36 alleviates PA-induced HMCs oxidative stress and fibrosis

Since several groups have reported that CD36 is involved in ECM deposition and oxidative stress, we further investigated the effect of CD36 inhibition on PA-induced oxidative stress and fibrosis. Using a BODIPY^{TM} lipid probe, we found that stimulation with PA increased FFA uptake in HMCs, which was verified by Oil Red O staining. However, sulfo-*N*-succinimidyl oleate (SSO), an inhibitor of CD36, reduced HMCs uptake of FFAs, which was also inhibited by 80 μM AS-IV; nevertheless, their combined use did not further increase this inhibition (Fig. 5). Furthermore, SSO suppressed FN, COL4 A1, TGF-β1, and p-smad2/3 expression following incubation of HMCs with PA for 24 h (Fig. 6). Similarly, SSO downregulated NOX4 and p22phox expression and reduced ROS production (Fig. 7); however, there were no significant differences between SSO and AS—IV alone and combined treatment (Figs. 6 and 7).

AS-IV suppresses CD36 upregulation in DN rats

We measured FFAs, blood sugar, and 24 h urine protein levels in rats to confirm success of the animal model (Table 1). The FFA level in the DN group was 5-fold higher than that in the Control group. Blood glucose and 24 h urine protein levels in the DN group were significantly higher than those in the Control group. These measured parameters proved the success of the animal model. Subsequently, to confirm the effect of ASIV on CD36 expression in DN rats, we evaluated CD36 expression by immunohistochemistry and western blotting. The immunohistochemistry results show that CD36 expression was significantly increased in DN rats, especially in the glomeruli, while 20–80 μM AS—IV markedly downregulated CD36 expression, which was verified by western blotting (Fig. 8).

Discussion

The present study investigated the effect of AS-IV on PA-induced HMCs fibrosis and oxidative stress and elucidated the underlying mechanisms. HMCs were exposed to PA for 24 h, followed by evaluation of fibrosis, oxidative stress, and intracellular lipid accumulation. We found that AS-IV attenuated PA-induced fibrosis and oxidative stress *via* the inhibition of CD36-mediated intracellular lipid deposition.

DN is the most serious chronic microvascular complication in DM. Metabolic changes in DM account for the pathophysiological processes of DN including mesangial ECM accumulation [2],

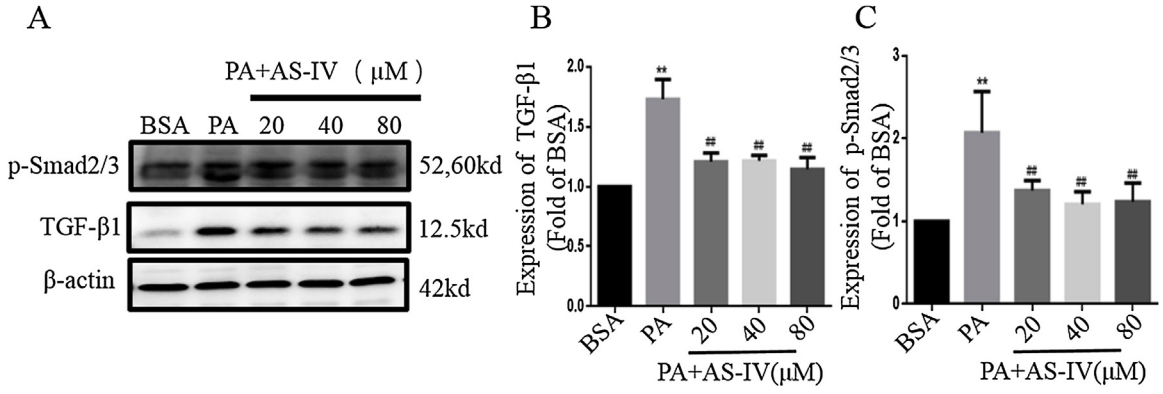

Fig. 2. AS-IV suppresses PA-induced TGF-β1 and p-Smad2/3 expression levels in HMCs. (A) TGF-β1 and p-Smad2/3 expression levels were detected by western blotting. (B) and (C) Densitometric analysis of TGF-β1 and p-Smad2/3 expression. Data are expressed as the mean ± SD of three independent experiments. $^{**}p < 0.01$ as compared with BSA; $^{\#\#}p < 0.01$ as compared with PA.

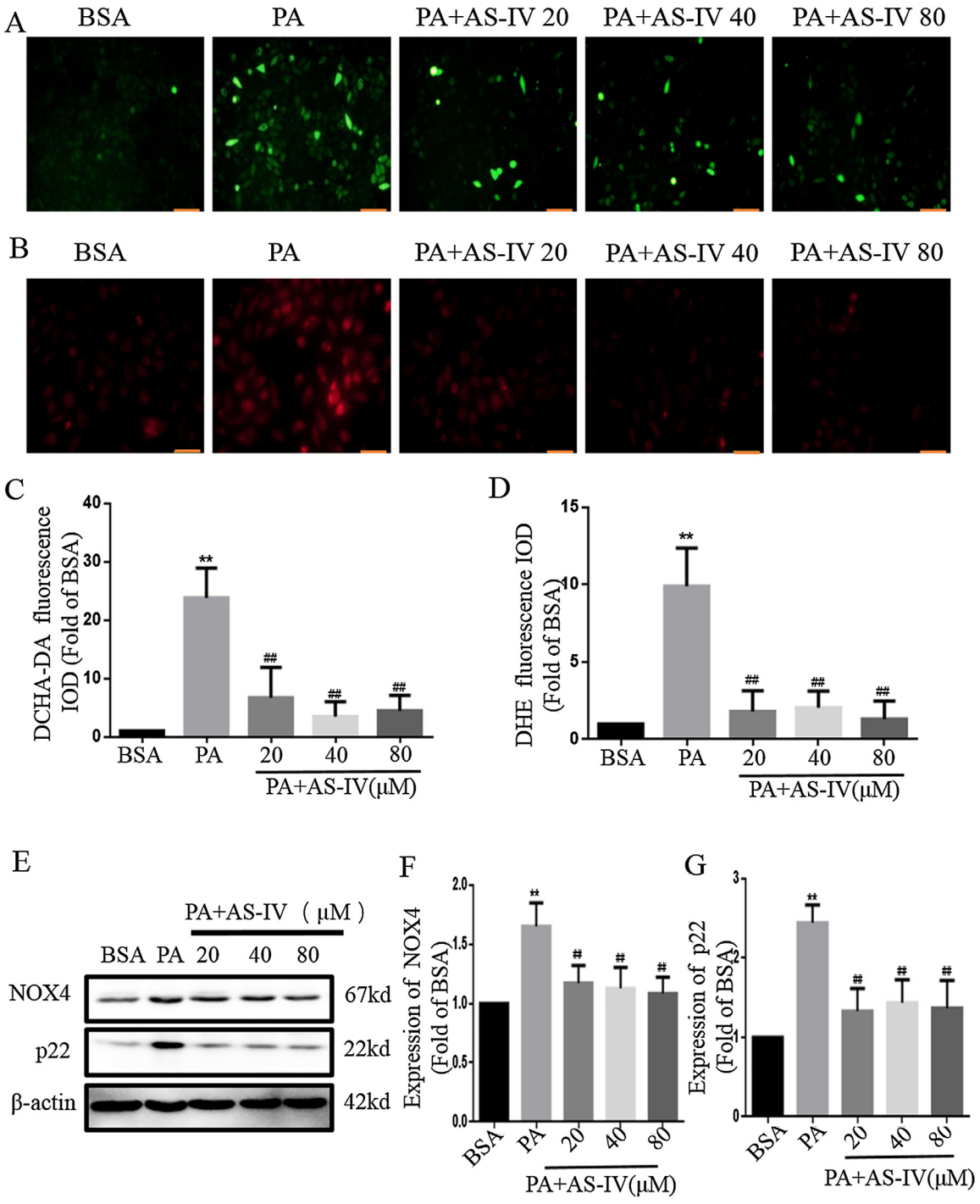

Fig. 3. AS-IV suppresses PA-induced ROS generation and NOX4 and p22phox expression in HMCs. (A) ROS levels were detected by the ROS-sensitive fluorescent probe, DCHA-DA (200×, bar = 50 μm). (B) ROS was detected by the ROS-sensitive fluorescent probe, DHE (400×, bar = 20 μm). (C) and (D) Average fluorescence intensity analysis of ROS generation. (E) NOX4 and p22phox expression levels were detected by western blotting. (F) and (G) Densitometric analysis of NOX4 and p22phox expression. Data are expressed as the mean ± SD of three independent experiments. $^{**}p < 0.01$ as compared with BSA; $^{\#\#}p < 0.01$ as compared with PA.

which is an important pathological change in DN, characterised by FN and Col4 deposition [27,28]. Excessive HMCs secretion of FN and Col4 is known to be due to activation of the TGF-β1/Smad2/3 pathway [29–31].

In addition to hyperglycemia, FFA levels are chronically elevated in DN. The concentration of FFAs in healthy individuals is 200–600 μM; however, this value increases by 4-fold in type 2 diabetes. PA is the most abundant saturated FFA, accounting for 25% of total fatty acids [15,32]. It has been shown that redundant PA plays an important role in insulin resistance, apoptosis, oxidative stress, and ECM accumulation [24,33,34]. PA is considered a risk factor of DN [35,36] and is commonly used for *in vitro* studies of DN [37–40]. According to the 'lipotoxicity' hypothesis, PA leads to kidney injury *via* increased accumulation of lipids. It has been previously reported that AS-IV suppresses PA-induced lipid accumulation [19]; thus, we hypothesised that AS-IV may improve HMCs fibrosis and oxidative stress induced by PA *via* the reduction of lipid accumulation. In the present study, both FN and Col4 A1

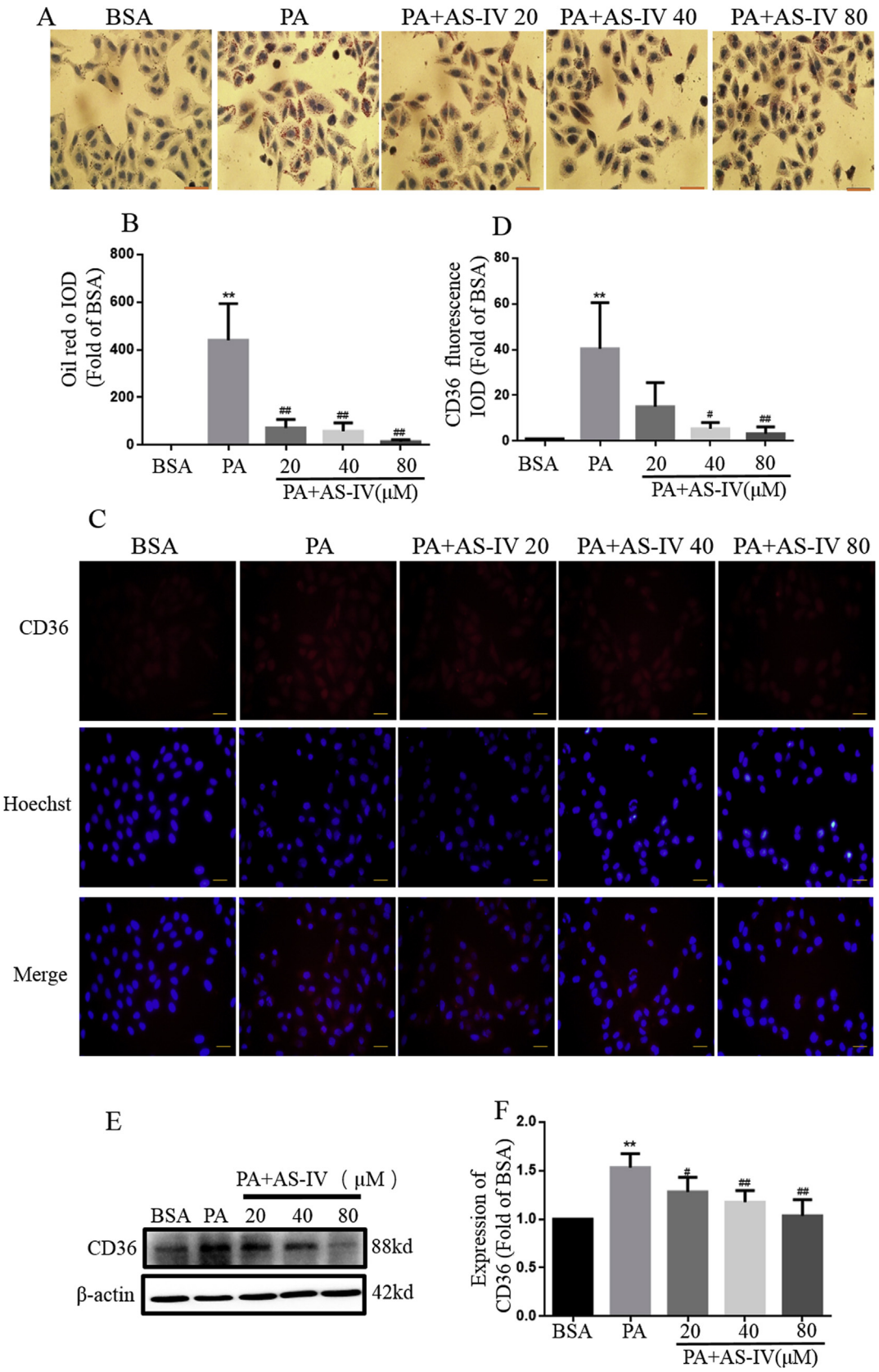

Fig. 4. AS-IV suppresses PA-induced lipid accumulation and CD36 expression in HMCs. (A) Cells were stained with Oil Red O (400 ×, bar = 20 μm). (B) Densitometric analysis of Oil Red O staining. (C) CD36 expression was detected by immunofluorescence (400×, bar = 20 μm). (D) Fluorescence intensity analysis of CD36 expression. (E) CD36 expression was detected by western blotting. (F) Densitometric analysis of CD36 expression. Data are expressed as the mean ± SD of three independent experiments. $^{**}p < 0.01$ as compared with BSA; $^{\#}p < 0.05$, $^{\#\#}p < 0.01$ as compared with PA.

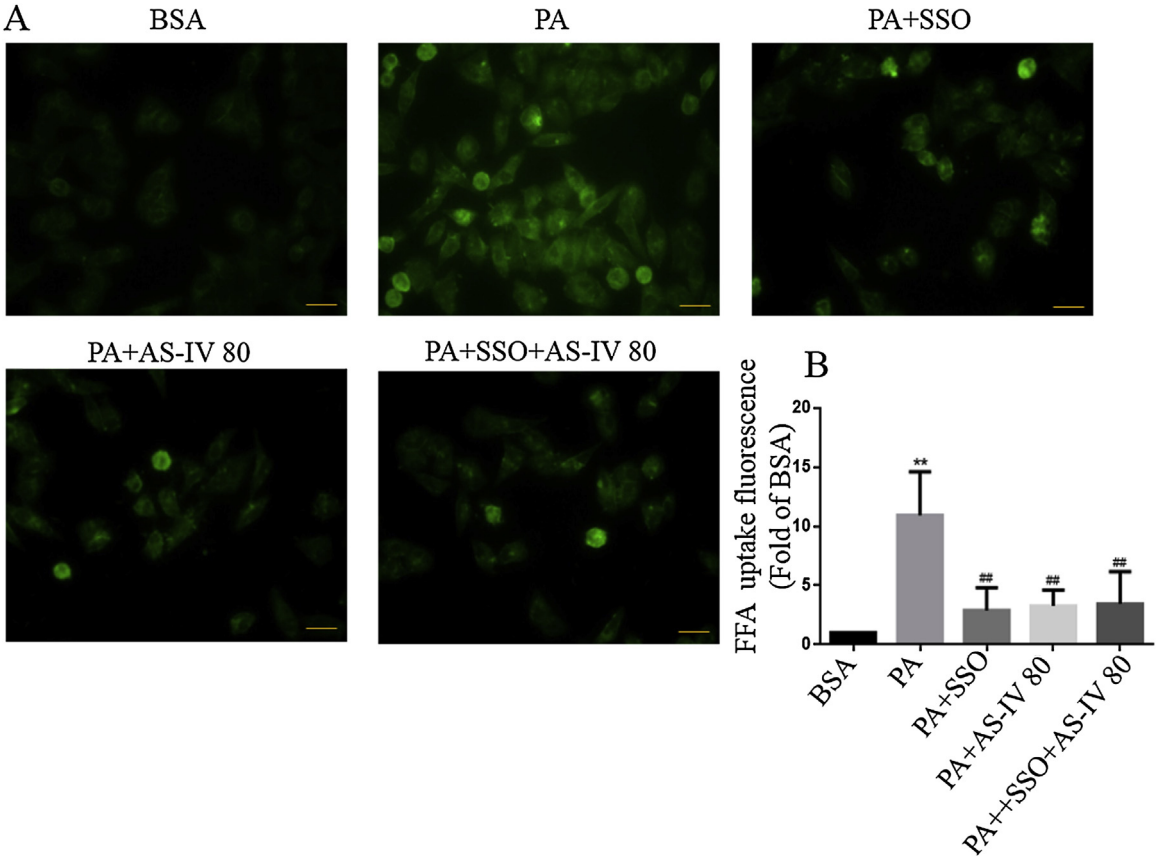

Fig. 5. AS-IV and the CD36 inhibitor, SSO, suppress PA-induced FFA uptake in HMCs. (A) The BODIPY^{TM} FL C16 lipid probe was used to measure FFA uptake (400×, bar = 20 μm). (B) Average fluorescence intensity analysis of FFA uptake. Data are expressed as the mean ± SD of three independent experiments. $^{**}p < 0.01$ as compared with BSA; $^{\#\#}p < 0.01$ as compared with PA.

expression increased significantly following stimulation of HMCs with PA for 24 h. The expression levels of activated TGF-β1 and p-Smad2/3 were consistent with those of FN and Col4 A1. Treatment with AS-IV attenuated HMCs fibrosis induced by PA and suppressed the activation of the TGF-β1/Smad2/3 pathway.

The deleterious role of ROS in DN has long been recognised, and the primary source of ROS in DN appears to be NOX4. Evidence suggests that NOX4 heterodimerisation with p22phox enhances the enzyme activity and/or stability without the requisite regulatory subunits [41]. NOX4 is associated with a variety of molecular events, in particular, interaction with the TGF-β1/Smad2/3 pathway, accelerating ECM deposition. Studies have demonstrated that TGF-ß1 increases the expression of NOX4 and ROS production. On the other hand, there is evidence suggesting that NOX4 has a potential role as an upstream mediator of TGF-β1/Smad2/3. For instance, NOX4-derived ROS generation leads to increased expression of TGF-β1 and FN, which is attenuated by the NOX inhibitor, GKT-136901. NOX4 and TGF-β1/Smad2/3 may form an amplification loop [10]. In the present study, the expression levels of NOX4 and p22phox increased significantly, in addition to ROS generation, in HMCs exposed to PA for 24 h. However, AS-IV inhibited ROS generation and reduced the expression of NOX4 and p22phox. These results provide evidence that AS-IV may exert an inhibitory effect on PA-induced HMCs fibrosis and oxidative stress.

CD36, a scavenger receptor, plays an important role in metabolic diseases including non-alcoholic fatty liver disease and diabetes mellitus [42,43]. The main function of CD36 is to mediate the uptake of medium- and long-chain fatty acids. Recently, CD36 has been considered an important therapeutic target for kidney disease, including DN [44]. In T2DM patients, soluble CD36 has a positive correlation with kidney markers such as urea, creatinine, and eGFR [45]. Noteworthy is that high glucose also increases the expression of CD36 [46,47]; thus, elevated blood glucose and PA induce CD36 expression in DM, especially in T2DM. It has been reported that knockdown of *CD36* prevents PA-dependent oxidative stress [11]. Moreover, Nath et al., have shown that PA uptake *via* CD36 promotes hepatocellular carcinoma epithelial-mesenchymal transition, including activation of TGF-β1/Smad2/3 [24]. This evidence suggests that CD36 may be a potential upstream mediator of NOX4 and TGF-β1.

In the present study, a DN model was induced by administration of an HFD and STZ, which is a widely used model of type 2 diabetic nephropathy. FFAs, blood glucose, and 24 h urine protein levels proved success of the animal model. Serum creatinine, urea nitrogen, and H&E and Masson staining were published in our previous study [23]. We found that CD36 expression was increased in the kidney of DN rats, especially in the glomeruli, and HMCs stimulated with PA. We hypothesised that excessive CD36 causes HMCs to absorb more free fatty acids, increasing intracellular lipid accumulation. FFA absorption experiments confirm our speculation that treatment with SSO significantly inhibits PA-induced FFA uptake in HMCs. Moreover, SSO also improved PA-induced fibrosis and oxidative stress; the fibrosis-associated protein, FN, Col4 A1, TGF-β1, and p-Smad2/3 were all downregulated, in addition to a reduction in NOX4 and p22phox expression and ROS generation. These results indicate a key role of CD36 in PA-induced fibrosis and oxidative stress. In the present study, we also examined the effect of AS-IV on the expression of CD36, and found that the increase in expression of CD36 was inhibited by AS-IV in both HMCs and DN

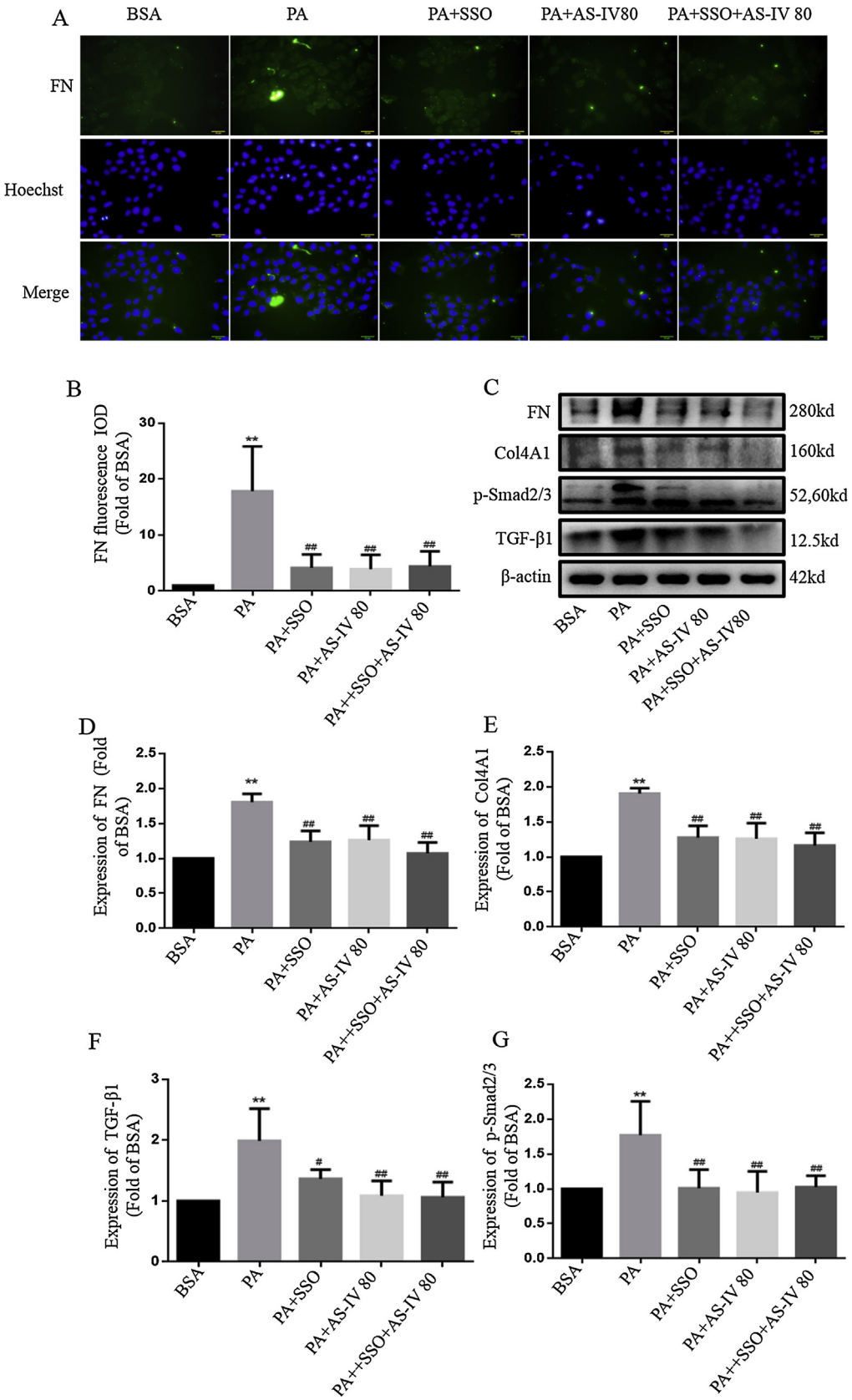

Fig. 6. The CD36 inhibitor, SSO, suppresses PA-induced fibrosis in HMCs. (A) FN expression was detected by immunofluorescence (400×, bar = 20 μm). (B) Analysis of FN expression. (C) FN, Col4 A1, TGF-β1, and p-Smad2/3 expression levels were detected by western blotting. (D–G) Densitometric analysis of FN, Col4 A1, TGF-β1, and p-Smad2/3 expression. Data are expressed as the mean ± SD of three independent experiments. $^{**}p < 0.01$ as compared with BSA; $^{\#}p < 0.05$, $^{\#\#}p < 0.01$ as compared with PA.

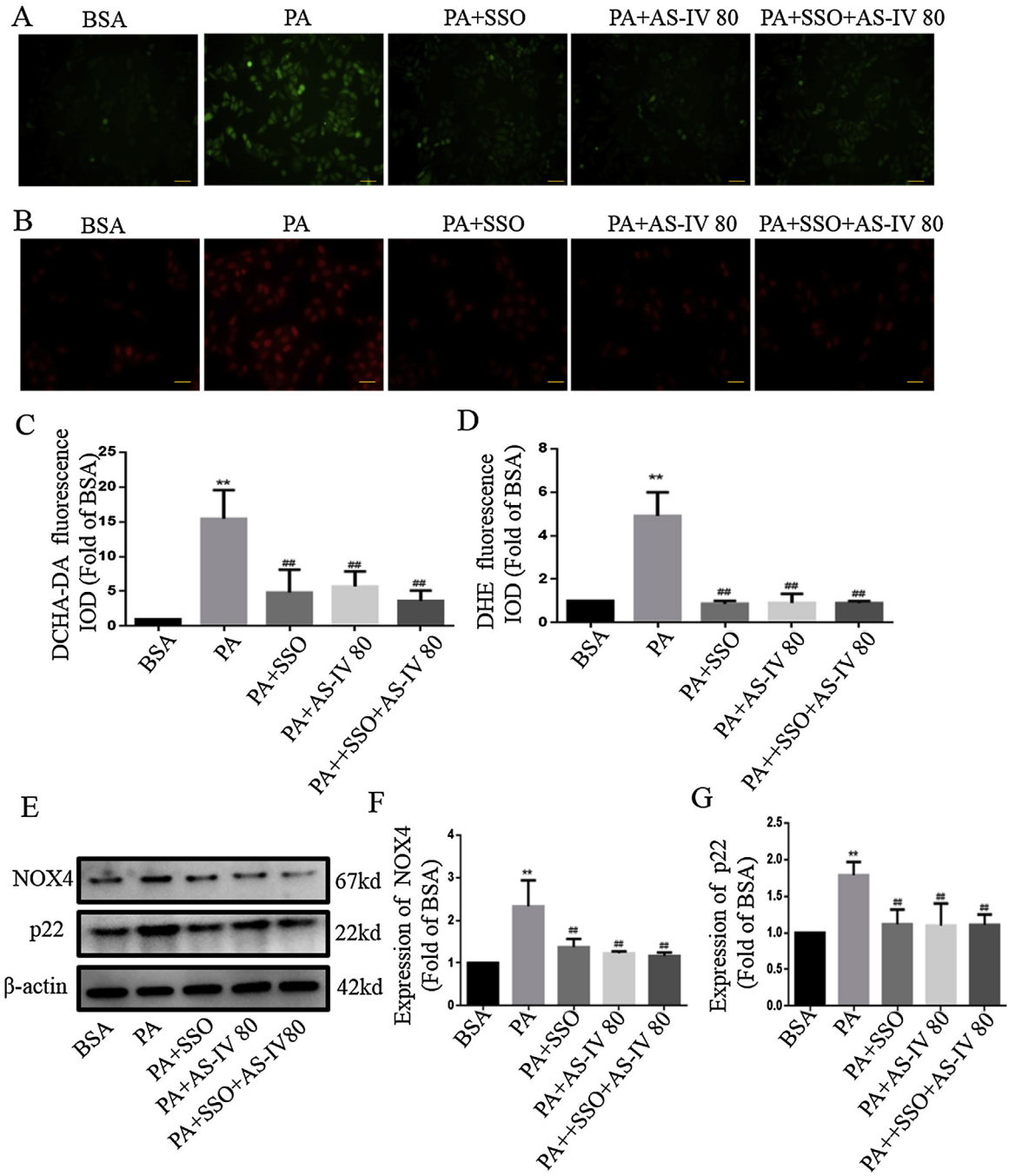

Fig. 7. The CD36 inhibitor, SSO, suppresses PA-induced oxidative stress in HMCs. (A) ROS levels were detected by the ROS-sensitive fluorescent probe, DCHA-DA (200×, bar = 50 μm). (B) ROS levels were detected using the ROS-sensitive fluorescent probe, DHE (400×, bar = 20 μm). (C) and (D) Average fluorescence intensity of ROS generation. (E) NOX4 and p22phox expression levels were detected by western blotting. (F) and (G) Densitometric analysis of NOX4 and p22phox expression. Data are expressed as the mean ± SD of three independent experiments. $^{**}p < 0.01$ as compared with BSA; $^{\#\#}p < 0.01$ as compared with PA.

Table 1
BG, FFA, and urine protein levels in DN rats (n = 6).

	CN	DN
BG (mmol/L)	5.2 ± 1.02	28.10 ± 1.76**
FFA (μmol/L)	571.43 ± 97.97	3051.02 ± 647.26**
Urine protein (mg/24 h)	9.06 ± 2.47	31.8 ± 4.17**

Data are expressed as the mean ± SD. $^{**}p < 0.01$ as compared with CN.

rats. Similarly, FFA uptake and lipid accumulation in HMCs were attenuated by AS-IV treatment; however, combined use of AS-IV and SSO did not enhance the therapeutic effect, suggesting that CD36 may be the target of AS-IV.

In conclusion, the present study indicates that PA induced HMCs fibrosis and oxidative stress by promoting CD36 expression, FFA uptake, and intracellular lipid accumulation. Treatment with AS-IV inhibited PA-induced fibrosis and oxidative stress via the downregulation of CD36 expression. Therefore, AS-IV may be a promising candidate for the prevention and treatment of early DN.

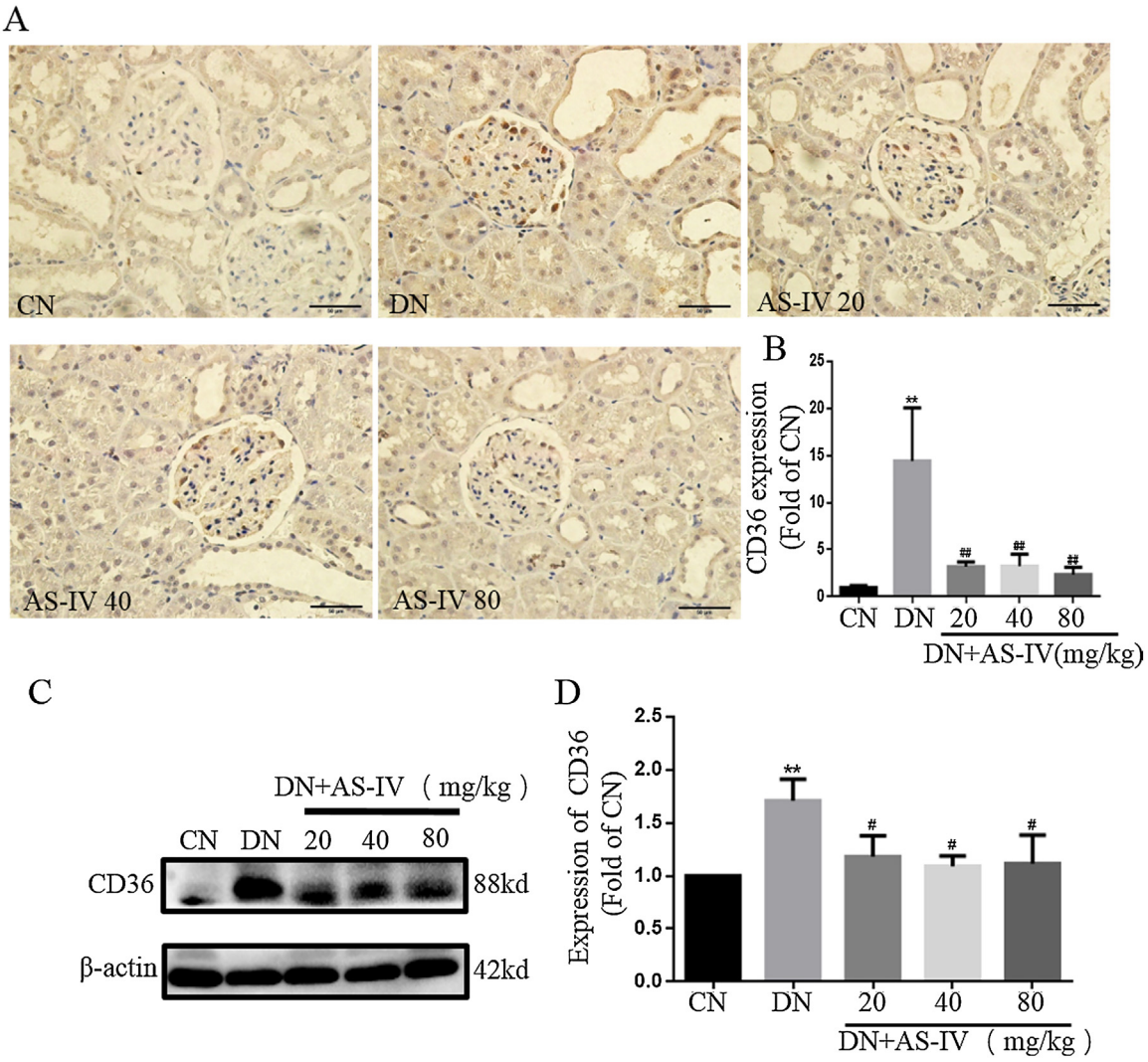

Fig. 8. AS-IV suppresses CD36 expression in DN rats. (A) CD36 expression was detected in the kidney by immunohistochemistry (400×, bar = 20 μm). (B) Quantitation of CD36 immunohistochemical staining. (C) CD36 expression was detected in the kidney by western blotting. (D) Densitometric analysis of CD36 expression. Data are expressed as the mean ± SD of three independent experiments. $^{**}p < 0.01$ as compared with CN; $^{\#}p < 0.05$, $^{\#\#}p < 0.01$ as compared with DN.

Declarations of interest

None.

Acknowledgments

This study was financially supported by grants from the Natural Science Foundation of Anhui Province Education Department (KJ2016SD35) and the National Nature Science Foundation of China (81671384). And thank Dake Huang and Li Gui (Synthetic Laboratory of Basic Medicine College, Anhui Medical University) for their excellent technical assistance.

References

[1] Guo H, Cao A, Chu S, Wang Y, Zang Y, Mao X, et al. Astragaloside IV attenuates podocyte apoptosis mediated by endoplasmic reticulum stress through upregulating sarco/endoplasmic reticulum Ca(2+)-ATPase 2 expression in diabetic nephropathy. Front Pharmacol 2016;7:500.
[2] Gnudi L, Coward RJM, Long DA. Diabetic nephropathy: perspective on novel molecular mechanisms. Trends Endocrinol Metab 2016;27(11):820–30.
[3] Miranda-Diaz AG, Pazarin-Villasenor L, Yanowsky-Escatell FG, Andrade-Sierra J. Oxidative stress in diabetic nephropathy with early chronic kidney disease. J Diabetes Res 2016;2016:7047238.
[4] Sifuentes-Franco S, Padilla-Tejeda DE, Carrillo-Ibarra S, Miranda-Diaz AG. Oxidative stress, apoptosis, and mitochondrial function in diabetic nephropathy. Int J Endocrinol 2018;2018:1875870.
[5] Rincon-Choles H, Kasinath BS, Gorin Y, Abboud HE. Angiotensin II and growth factors in the pathogenesis of diabetic nephropathy. Kidney Int Suppl 2002;2011(82):S8–11.
[6] Gorin Y, Block K. Nox as a target for diabetic complications. Clin Sci 2013;125(8):361–82.
[7] Sun L, Li W, Li W, Xiong L, Li G, Ma R. Astragaloside IV prevents damage to human mesangial cells through the inhibition of the NADPH oxidase/ROS/Akt/NFkappaB pathway under high glucose conditions. Int J Mol Med 2014;34(1):167–76.
[8] Wan RJ, Li YH. MicroRNA146a/NAPDH oxidase4 decreases reactive oxygen species generation and inflammation in a diabetic nephropathy model. Mol Med Rep 2018;17(3):4759–66.
[9] Gorin Y, Block K. Nox4 and diabetic nephropathy: with a friend like this, who needs enemies? Free Radic Biol Med 2013;61:130–42.
[10] Jiang F, Liu GS, Dusting GJ, Chan EC. NADPH oxidase-dependent redox signaling in TGF-beta-mediated fibrotic responses. Redox Biol 2014;2:267–72.
[11] Ly LD, Xu S, Choi SK, Ha CM, Thoudam T, Cha SK, et al. Oxidative stress and calcium dysregulation by palmitate in type 2 diabetes. Exp Mol Med 2017;49(2):e291.
[12] Spiller S, Bluher M, Hoffmann R. Plasma levels of free fatty acids correlate with type 2 diabetes mellitus. Diabetes Obes Metab 2018;20(11):2661–9.
[13] Kuwagata S, Kume S, Chin-Kanasaki M, Araki H, Araki S, Nakazawa J, et al. MicroRNA148b-3p inhibits mTORC1-dependent apoptosis in diabetes by repressing TNFR2 in proximal tubular cells. Kidney Int 2016;90(6):1211–25.
[14] Yasuda M, Tanaka Y, Kume S, Morita Y, Chin-Kanasaki M, Araki H, et al. Fatty acids are novel nutrient factors to regulate mTORC1 lysosomal localization and apoptosis in podocytes. Biochim Biophys Acta 2014;1842(7):1097–108.

[15] Xu S, Nam SM, Kim JH, Das R, Choi SK, Nguyen TT, et al. Palmitate induces ER calcium depletion and apoptosis in mouse podocytes subsequent to mitochondrial oxidative stress. Cell Death Dis 2015;6:e1976.
[16] Mishra R, Simonson MS. Oleate induces a myofibroblast-like phenotype in mesangial cells. Arterioscler Thromb Vasc Biol 2008;28(3):541–7.
[17] Koyama T, Kume S, Koya D, Araki S, Isshiki K, Chin-Kanasaki M, et al. SIRT3 attenuates palmitate-induced ROS production and inflammation in proximal tubular cells. Free Radic Biol Med 2011;51(6):1258–67.
[18] Li L, Hou X, Xu R, Liu C, Tu M. Research review on the pharmacological effects of astragaloside IV. Fundam Clin Pharmacol. 2017;31(1):17–36.
[19] Zhou B, Zhou DL, Wei XH, Zhong RY, Xu J, Sun L. Astragaloside IV attenuates free fatty acid-induced ER stress and lipid accumulation in hepatocytes via AMPK activation. Acta Pharmacol Sin 2017;38(7):998–1008.
[20] Qiu YY, Tang LQ, Wei W. Berberine exerts renoprotective effects by regulating the AGEs-RAGE signaling pathway in mesangial cells during diabetic nephropathy. Mol Cell Endocrinol 2017;443:89–105.
[21] Mishra R, Simonson MS. Saturated free fatty acids and apoptosis in microvascular mesangial cells: palmitate activates pro-apoptotic signaling involving caspase 9 and mitochondrial release of endonuclease G. Cardiovasc Diabetol 2005;4:2.
[22] Zezina E, Snodgrass RG, Schreiber Y, Zukunft S, Schurmann C, Heringdorf DMZ, et al. Mitochondrial fragmentation in human macrophages attenuates palmitate-induced inflammatory responses. Biochim Biophys Acta 2018;1863(4):433–46.
[23] Ju Y, Su Y, Chen Q, Ma K, Ji T, Wang Z, et al. Protective effects of Astragaloside IV on endoplasmic reticulum stress-induced renal tubular epithelial cells apoptosis in type 2 diabetic nephropathy rats. Biomed Pharmacother 2018;109:84–92.
[24] Nath A, Li I, Roberts LR, Chan C. Elevated free fatty acid uptake via CD36 promotes epithelial-mesenchymal transition in hepatocellular carcinoma. Sci Rep 2015;5:14752.
[25] Ben-Harosh Y, Anosov M, Salem H, Yatchenko Y, Birk R. Pancreatic stellate cell activation is regulated by fatty acids and ER stress. Exp Cell Res 2017;359(1):76–85.
[26] Iio A, Ito M, Itoh T, Terazawa R, Fujita Y, Nozawa Y, et al. Molecular hydrogen attenuates fatty acid uptake and lipid accumulation through downregulating CD36 expression in HepG2 cells. Med Gas Res 2013;3(1):6.
[27] Chen P, Shi X, Xu X, Lin Y, Shao Z, Wu R, et al. Liraglutide ameliorates early renal injury by the activation of renal FoxO1 in a type 2 diabetic kidney disease rat model. Diabetes Res Clin Pract 2018;137:173–82.
[28] Zhang L, Chen Z, Gong W, Zou Y, Xu F, Chen L, et al. Paeonol ameliorates diabetic renal fibrosis through promoting the activation of the Nrf2/ARE pathway via Up-Regulating Sirt1. Front Pharmacol 2018;9:512.
[29] Chen L, Li L, Chen J, Li L, Zheng Z, Ren J, et al. Oleoylethanolamide, an endogenous PPAR-alpha ligand, attenuates liver fibrosis targeting hepatic stellate cells. Oncotarget 2015;6(40):42530–40.
[30] Zhang R, Li J, Huang T, Wang X. Danggui buxue tang suppresses high glucose-induced proliferation and extracellular matrix accumulation of mesangial cells via inhibiting lncRNA PVT1. Am J Transl Res 2017;9(8):3732–40.
[31] Jie L, Pengcheng Q, Qiaoyan H, Linlin B, Meng Z, Fang W, et al. Dencichine ameliorates kidney injury in induced type II diabetic nephropathy via the TGF-beta/Smad signalling pathway. Eur J Pharmacol 2017;812:196–205.
[32] Sieber J, Jehle AW. Free Fatty acids and their metabolism affect function and survival of podocytes. Front Endocrinol (Lausanne). 2014;5:186.
[33] Sun P, Zeng Q, Cheng D, Zhang K, Zheng J, Liu Y, et al. Caspase recruitment domain protein 6 protects against hepatic steatosis and insulin resistance by suppressing apoptosis signal-regulating kinase 1. Hepatology 2018;68(6):2212–29.
[34] Natalicchio A, Labarbuta R, Tortosa F, Biondi G, Marrano N, Peschechera A, et al. Exendin-4 protects pancreatic beta cells from palmitate-induced apoptosis by interfering with GPR40 and the MKK4/7 stress kinase signalling pathway. Diabetologia 2013;56(11):2456–66.
[35] Jia G, Di F, Wang Q, Shao J, Gao L, Wang L, et al. Non-alcoholic fatty liver disease is a risk factor for the development of diabetic nephropathy in patients with type 2 diabetes mellitus. PLoS One 2015;10(11)e0142808.
[36] Han LD, Xia JF, Liang QL, Wang Y, Wang YM, Hu P, et al. Plasma esterified and non-esterified fatty acids metabolic profiling using gas chromatography-mass spectrometry and its application in the study of diabetic mellitus and diabetic nephropathy. Anal Chim Acta 2011;689(1):85–91.
[37] Yao F, Li Z, Ehara T, Yang L, Wang D, Feng L, et al. Fatty Acid-Binding Protein 4 mediates apoptosis via endoplasmic reticulum stress in mesangial cells of diabetic nephropathy. Mol Cell Endocrinol 2015;411:232–42.
[38] Lee E, Lee HS. Peroxidase expression is decreased by palmitate in cultured podocytes but increased in podocytes of advanced diabetic nephropathy. J Cell Physiol 2018;233(12):9060–9.
[39] Huang CN, Wang CJ, Yang YS, Lin CL, Peng CH. Hibiscus sabdariffa polyphenols prevent palmitate-induced renal epithelial mesenchymal transition by alleviating dipeptidyl peptidase-4-mediated insulin resistance. Food Funct 2016;7(1):475–82.
[40] Han E, Shin E, Kim G, Lee JY, Lee YH, Lee BW, et al. Combining SGLT2 inhibition with a thiazolidinedione additively attenuate the very early phase of diabetic nephropathy progression in type 2 diabetes mellitus. Front Endocrinol (Lausanne). 2018;9:412.
[41] Zana M, Peterfi Z, Kovacs HA, Toth ZE, Enyedi B, Morel F, et al. Interaction between p22(phox) and Nox4 in the endoplasmic reticulum suggests a unique mechanism of NADPH oxidase complex formation. Free Radic Biol Med 2018;116:41–9.
[42] He J, Lee JH, Febbraio M, Xie W. The emerging roles of fatty acid translocase/CD36 and the aryl hydrocarbon receptor in fatty liver disease. Exp Biol Med (Maywood) 2011;236(10):1116–21.
[43] Marechal L, Laviolette M, Rodrigue-Way A, Sow B, Brochu M, Caron V, et al. The CD36-PPARgamma pathway in metabolic disorders. Int J Mol Sci 2018;19(5):1529.
[44] Yang X, Okamura DM, Lu X, Chen Y, Moorhead J, Varghese Z, et al. CD36 in chronic kidney disease: novel insights and therapeutic opportunities. Nat Rev Nephrol 2017;13(12):769–81.
[45] Ekici M, Kisa U, Arikan Durmaz S, Ugur E, Nergiz-Unal R. Fatty acid transport receptor soluble CD36 and dietary fatty acid pattern in type 2 diabetic patients: a comparative study. Br J Nutr 2018;119(2):153–62.
[46] Feng L, Gu C, Li Y, Huang J. High glucose promotes CD36 expression by upregulating peroxisome proliferator-activated receptor gamma levels to exacerbate lipid deposition in renal tubular cells. Biomed Res Int 2017;2017:1414070.
[47] Song KH, Park J, Ha H. High glucose increases mesangial lipid accumulation via impaired cholesterol transporters. Transplant Proc 2012;44(4):1021–5.